FVTD Thin-Wire Modelling of a Microwave Tomography System

Dmitry Firsov, Cam Kaye and Joe LoVetri

Department of Electrical and Computer Engineering
University of Manitoba, Winnipeg, Manitoba, Canada R3T 5V6
firsovd@ee.umanitoba.ca, umkayecj@cc.umanitoba.ca, Joe_LoVetri@UManitoba.ca

Abstract: The finite-volume time-domain (FVTD) method with an appropriate thin-wire modeling capability is used for a preliminary investigation of a class of resonant-chamber microwave tomography systems. A mathematical model in which an arbitrarily oriented thin-wire, discretized via line-elements, is placed in the unstructured FVTD mesh and coupled to the 2nd-order- accurate flux-split upwind time-domain electromagnetic field algorithm is presented. The wires can be terminated by lumped-element Thèvenin sources. The thin-wire model has been validated against several test cases and results for three of these are shown herein: a dipole and monopole in free space, and a resonant chamber excited by a coaxial cable. Results for the field distribution in a resonant-chamber microwave tomography (MWT) system are then given. The system consists of a capped cylindrical resonant chamber excited by various dipole configurations including resistively-loaded dipoles. The same dipoles are used for the receiving elements.

Keywords: Thin-wire modelling, finite-volume time-domain (FVTD), upwind flux-split scheme, Maxwell's equations, microwave tomography (MWT).

1. Introduction

The efficient use of electromagnetic modelling algorithms, such as the finite-difference, finite-element, and finite-volume time-domain (hereafter FDTD, FETD, and FVTD) methods, depends on good source and electronic component sub-grid models, so that fine geometries don't need to be resolved by the mesh itself. One of the most important and most natural geometries that one needs to model are thin wires and electrical lumped elements attached to these wires. One technique that has been developed for modelling thin wires in FVTD is due to Bonnet *et al.* [1] where a wire, of arbitrary radius a, is located along the long edge of a set of prismatic elements surrounding the wire. This technique uses a time-space interlaced mesh to update the charge and current on the wire. Although the reported results are good, the use of prismatic elements for modelling thin wires generally makes the technique cumbersome to use, and more importantly, it is not clear how one would go about modelling *Y*-junctions between several thin wires using such prismatic elements. It is more convenient to have a method of modelling thin wires that can locate the wires at any arbitrary location and orientation within the FVTD mesh. This has been recently accomplished for FETD and FDTD by Edelvik *et al.* [2, 3].

The FVTD method we use is similar to the one described by Bonnet *et al.* [1] and details specific to our method can be found in [4]. In this paper we describe how we've adapted Edelvik's thin-wire model to our FVTD algorithm. Briefly, the Holland-Simpson model [5] for a thin-wire results in transmission-line equations for the voltage and current on the wire. The wire current is projected onto the FVTD grid as a distributed current source and the longitudinal electric field around the wire is projected along the wire as a distributed voltage-source term in the transmission-line equations. The thin-wire transmission-line equations are solved using a specially developed upwinding algorithm for the collocated voltage and current variables on the wire (discretized into one-dimensional elements). To avoid numerical oscillations on the wire, a flux-limiting procedure is used. The space-time updating algorithm for the thin-wire model was

chosen to be equivalent in structure to the updating algorithm of the FVTD scheme; thus, the software implementation of the two methods is simplified. Lumped element Thèvenin source boundary conditions are used to terminate the transmission-line equations. This allows one to excite the wires using lumped-element sources. Results are shown for three test problems—a dipole and monopole in free space, and a resonant chamber excited by a coaxial cable—and validated against results presented in previous publications using different numerical methods (FDTD and FETD). Our algorithm demonstrates good agreement with numerical and experimental results published by other authors.

Finally, we investigate the use of our FVTD thin-wire code for the simulation of a resonant-cavity microwave tomography (MWT) system that we are developing. We show preliminary results of the field distributions inside the resonant cavity associated with various configurations of dipole sources (*v*-shaped and resistively-loaded dipoles). The array of dipoles act both as transmitters and receivers of electromagnetic energy. These results are only preliminary; the main purpose of this paper is to demonstrate the use of the FVTD thin-wire code in the design of complicated electromagnetic systems.

2. Thin-Wire Modelling in the Finite-Volume Method

First, consider the fields around an infinitely long thin-wire of radius a running in the $\hat{\boldsymbol{l}}$ direction. In cylindrical coordinates, with the assumption that the electromagnetic fields E_r and H_ϕ are proportional to $1/r$ close to the thin-wire, the voltage and current on the wire can be written in generalized-vector form as

$$\boldsymbol{u}_t + A\boldsymbol{u}_x + B\boldsymbol{u} = \boldsymbol{s} \tag{1}$$

where the solution vector is $\boldsymbol{u} = (V, I)^T$, with $V(x, t)$ and $I(x, t)$ are the voltage and current variables along the transmission line. (Subscripts on these variables denote differentiation with respect to the subscripted variable.) The coefficient matrices are given by

$$A = \begin{bmatrix} 0 & C^{-1} \\ L^{-1} & 0 \end{bmatrix}, \; B = \begin{bmatrix} C^{-1}G & 0 \\ 0 & L^{-1}R \end{bmatrix} \tag{2}$$

where C, L, G, and R are the per-unit capacitance, inductance, conductance, and resistance of the line, and the source vector $\boldsymbol{s} = (0, L^{-1}E_l)^T$, and E_l represent the longitudinal electric field along the line. The wire inductance is computed as $L = (\mu/2\pi)\ln[(r_0 + a)/2a]$ (see [2, 3]), $C = \varepsilon\mu/L$ and $G = C\sigma/\varepsilon$. The variable r_0 is the radius of influence of the wire onto the space surrounding it. To approximate system (1) the wire is split into segments l_i, $i = 1,...,N$. Each wire segment can be arbitrarily oriented with respect to the FVTD mesh.

The fields in the space around the wire, which are calculated by the FVTD method, must be coupled to the current and voltage on the wire. In [2] and [3] Edelvik *et al.* presented a new technique for implementing this coupling. The method is based on using an effective longitudinal electric field E_l as a source term in (1), in addition to an effective current density in Maxwell's equations due to the current on the wire. For the computation of these effective quantities, we make use of Edelvik's weighting function $g(r)$ which is given by the expression

$$g(r) = \left(1 + \cos\frac{\pi r}{r_0}\right) \Big/ \left(\pi(r_0^2 - a^2) - \frac{2r_0^2}{\pi}\left(1 + \cos\frac{\pi a}{r_0} + \frac{\pi a}{r_0}\sin\frac{\pi a}{r_0}\right)\right), \tag{3}$$

for $a \le r \le r_0$ and zero otherwise, where r is the perpendicular distance from the wire segment. This weighting function satisfies the special condition

$$\int_{r \ge a} g(r) 2\pi r dr = 1. \tag{4}$$

We can now denote the volume of the cylinder of radius r_0 around the wire segment l_i as C_i and this generates a set of elements of the FVTD mesh that intersect with the cylindrical volume: $S_i = \{T_j : T_j \cap C_i \neq \varnothing\}$. As in [2] and [3] we can now calculate the effective longitudinal electric field E_l along the wire segment as

$$[E_l]_i = \frac{1}{h_i}\int_{C_i} \hat{\boldsymbol{l}}_i \cdot \boldsymbol{E}(\boldsymbol{x}) g(r(\boldsymbol{x}))\, d\boldsymbol{x} = \frac{1}{h_i}\sum_{T_j \in S_i T_j} \int \hat{\boldsymbol{l}}_i \cdot \boldsymbol{E}(\boldsymbol{x}) g(r(\boldsymbol{x}))\, d\boldsymbol{x}, \tag{5}$$

where h_i is the length of wire segment l_i, the unit vector along the wire is $\hat{\boldsymbol{l}}_i$, and the function $r(\boldsymbol{x})$ denotes the perpendicular distance from the wire segment to a point $\boldsymbol{x}$.

In [3] it was suggested to take r_0 to be 1.7Δ, where Δ is the average edge-length of tetrahedrals containing the wire. In our FVTD method, we modify this formula slightly by choosing r_0 to be $3\Delta_c$ where Δ_c is an average of the distance from the barycentres of all the elements containing the centroids of the wire segments to the barycentres of all the neighbouring elements. The integral (5) is computed with the 5^{th} order Gaussian quadrature rules. The $\boldsymbol{E}(\boldsymbol{x})$ field was calculated at the quadrature points on elements T_j in the same manner as the fluxes were interpolated.

The same weighting function, $g(\cdot)$, was used to create an effective current density $\boldsymbol{J}$ around the wire from the current on the wire. The current density $\boldsymbol{J}$ is kept parallel to each wire segment and computed on each cell that intersects the cylinder of the radius r_0 around the wire segment l_i (*i.e.,* $\forall T_j \in S_i$). According to [3], for the $\boldsymbol{J}_j^i$ on each element $T_j \in S_i$ we have

$$\boldsymbol{J}_j^i = I_i \hat{\boldsymbol{l}}_i \int_{T_j} g(r(\boldsymbol{x}))\, dx, \tag{6}$$

where I_i is the current on wire segment l_i.

At the terminations of the line, boundary conditions need to be specified that relate the voltage and current variables. For a Thèvenin voltage source, $V^{\text{th}}(t)$, at the near-end of the line, $x = 0$, we have the linear relationship $V(0, t) + R^{\text{th}} I(0, t) = V_s^{\text{th}}(t)$ where R^{th} specifies the Thèvenin resistance. On each wire segment l_i having the length h_i we can define the average value of the solution vector as

$$\boldsymbol{u}_i \triangleq \frac{1}{h_i}\int_{x_i - h_i/2}^{x_i + h_i/2} \boldsymbol{u}\, dx \tag{7}$$

where x_i is the centroid of the segment. Integrating (1) over an arbitrary segment, we get

$$\boldsymbol{u}_i + \frac{1}{h_i}\int_{x_i - h_i/2}^{x_i + h_i/2} A\boldsymbol{u}_x dx + \frac{1}{h_i}\int_{x_i - h_i/2}^{x_i + h_i/2} B\boldsymbol{u}\, dx = \frac{1}{h_i}\int_{x_i - h_i/2}^{x_i + h_i/2} \boldsymbol{s}\, dx \triangleq \boldsymbol{s}_i. \tag{8}$$

The integration over each wire segment can be written as

$$(A\boldsymbol{u}_x)_i \triangleq \frac{1}{h_i}\int_{x_i - h_i/2}^{x_i + h_i/2} A\boldsymbol{u}_x dx = \frac{1}{h_i}\sum_{k=-1,\, k\neq 0}^{1} A(k)\boldsymbol{u}_{i+k/2},\ A(k) = k\begin{bmatrix} 0 & C^{-1} \\ L^{-1} & 0 \end{bmatrix} = kA, \tag{9}$$

where the sum represents a sum over the "facets" of the line-segment. The constant k plays the same role as the normal to the facet in our 3-D FVTD code [4]. The evaluation of $\boldsymbol{u}$ at the end-points of each line-segment, $\boldsymbol{u}_{i+k/2}$, is performed using a similar flux-splitting technique as in the FVTD algorithm. We decompose A into positive and negative matrices as $A(k) = A^{+}(k) + A^{-}(k)$, corresponding to the positive and negative eigenvalue decomposition. These can be written succinctly as

$$A^{\pm}(k) = \frac{1}{2}\begin{bmatrix} \pm v & kC^{-1} \\ kL^{-1} & \pm v \end{bmatrix}. \tag{10}$$

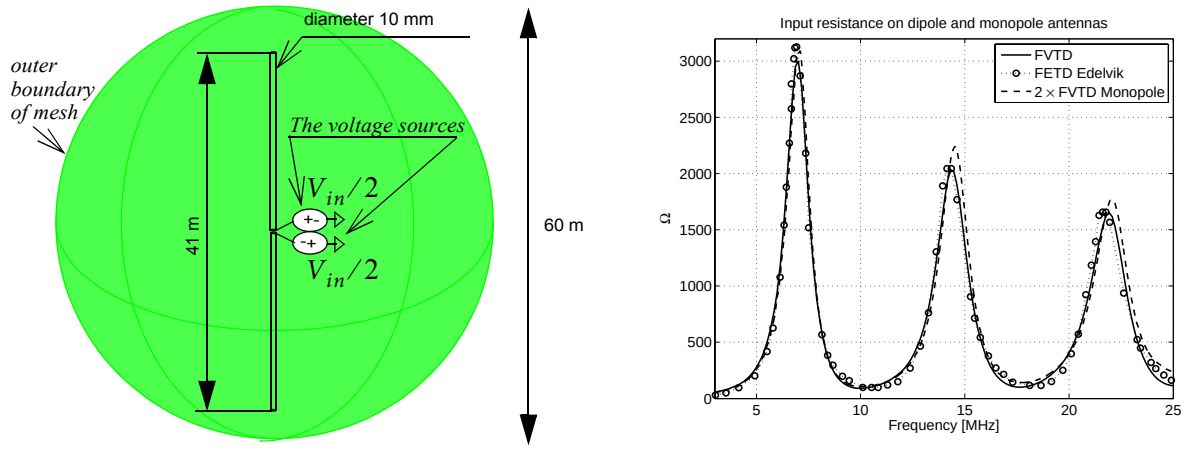

Figure 1. Comparison of the input resistance of the monopole and dipole antennas with results given in [3].

With this flux-splitting we can write (9) as

$$(A\boldsymbol{u}_x)_i \approx \frac{1}{h_i} \sum_{k=-1,\,k\neq 0}^{1} (A^{+}(k)\boldsymbol{u}^{+}_{i+k/2} + A^{-}(k)\boldsymbol{u}^{-}_{i+k/2}), \tag{11}$$

where $\boldsymbol{u}^{+}_{i+k/2}$ is the interpolated solution value computed from the inside of wire segment i, and $\boldsymbol{u}^{-}_{i+k/2}$ is the interpolated solution value computed from the inside of wire segment $i+k$ (that is, computed from the neighbouring element).

3. Thin-Wires Test Problems

Results for three test problems are now shown as a validation of the thin-wire formulation. All results were obtained using Gmsh® to generate tetrahedral meshes and our in-house FVTD engine.

i) Antenna dipole and antenna monopole

A simple antenna dipole and monopole as modelled in [3] are considered first. The length of the antenna dipole is 41 meters with a diameter of 10 mm. The dipole is modelled as two thin wires connected in the centre by two terminal points as shown in Fig. 1. Two voltage sources are applied to the two terminal points. The voltage source was imposed on the terminal as the derivative of a Gaussian with parameters $b = 2\times10^{-8}$ and $t_0 = 1.2\times10^{-7}$. We segmented the wire with elements having an average segment size of 2 metres. The space around the wire was partitioned by tetrahedrons with an average edge size of about 1 metre. A monopole above a PEC ground plane was modelled in a similar way. The current at the centre of the first segment next to the voltage source terminal was stored, allowing us to calculate the input impedance for the dipole antenna. The results were compared with those presented in [3] (shown in Fig. 1.)

ii) Shielded-enclosure test case

As the third validation, the example found in [2] and [3] for a thin-wire exciting a resonant cavity is presented. The geometry of the problem is shown in Fig. 2. The input source was modelled at the top terminal of the thin-wire using a Thèvenin voltage source with output resistance equal to 50 Ω. The wire is terminated at the bottom by a 47 Ω resistor. The input power is calculated as $P = 0.5Re[(V_0 I_0^*)/|\tilde{V}_{in}|^2]$, where V_0 and I_0 are the voltage and current at the input terminal, and V_{in} is the input voltage, set as a Gaussian modulated cosine $V_{in}(t) = \cos(2\pi f(t-t_0))\exp[-(t-t_0)^2/b^2]$, where $f = 1.15GHz$, $b = 5\times10^{-10}$, and $t = 2.8211\times10^{-9}$ sec. As can be seen in Fig. 2, the FVTD gives similar results for low frequencies, but some numerical dissipation at high frequencies is visible.

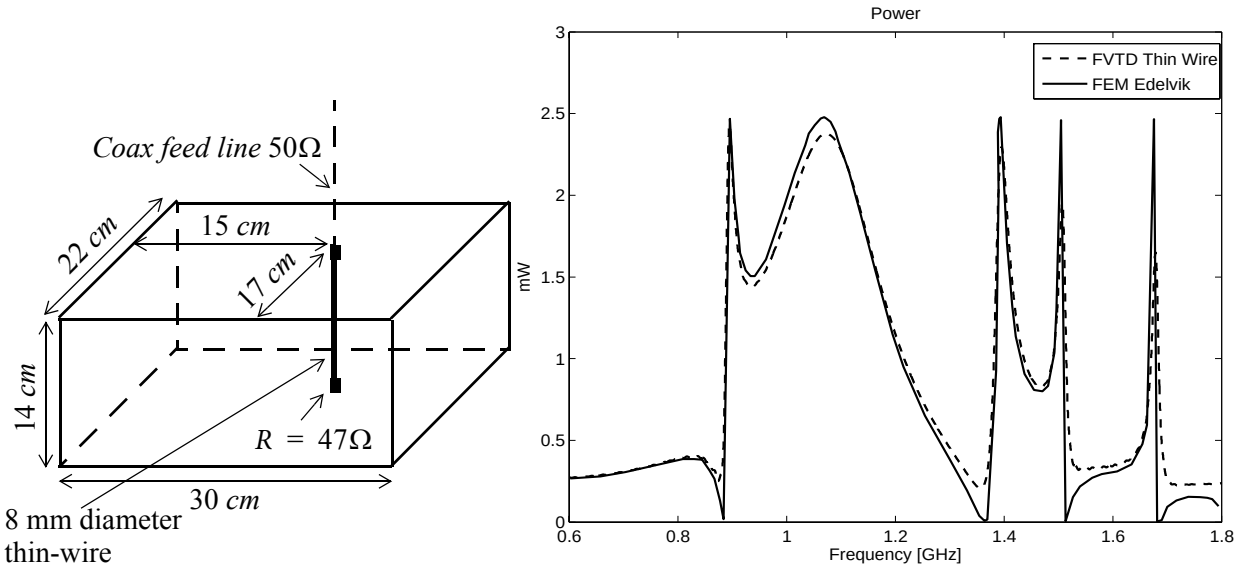

Figure 2. Geometry of resonant enclosure & power delivered to load compared with [3].

iii) Resonant-chamber microwave tomography system

A necessary step in the development of our own microwave tomographic imaging system involves the simulation and modeling of the antenna array and the imaging chamber itself. The ultimate criterion for the design of the antenna to be used in the physical prototype is to maximize the amount of energy transmitted directly across the center of the cylinder to the receiving antennas at the opposite side (in the same plane) while maintaining a flat profile for E_z in the 2D imaging plane at the level of the antennas. We created a mesh of tetrahedral elements representing a physical model of a cylindrical PEC-walled imaging chamber thirty centimeters in diameter and height. The chamber contains twenty-four dipole antennas spaced evenly around the circumference of the cylinder, as shown in Fig. 3. The antennas were placed at an offset of a quarter-wavelength (at the centre frequency of a Gaussian-modulated sinusoidal source) from the PEC walls to allow for reflective reinforcement of the energy emitted by the antennas. Furthermore, purely for simulation purposes, a coupling medium having a dielectric constant of 15 was used to fill the volume of the chamber. Finally, the top and the bottom of the chamber were capped with ovoidal surfaces, giving the model a pill-shaped appearance. These caps were modeled both as PEC or absorbing boundaries in various comparative trials. Two antenna geometries were simulated and compared: the straight half-wavelength dipole, and the half-wavelength 90° vee-dipole (both having 1 mm radii). For both cases, PEC as well as

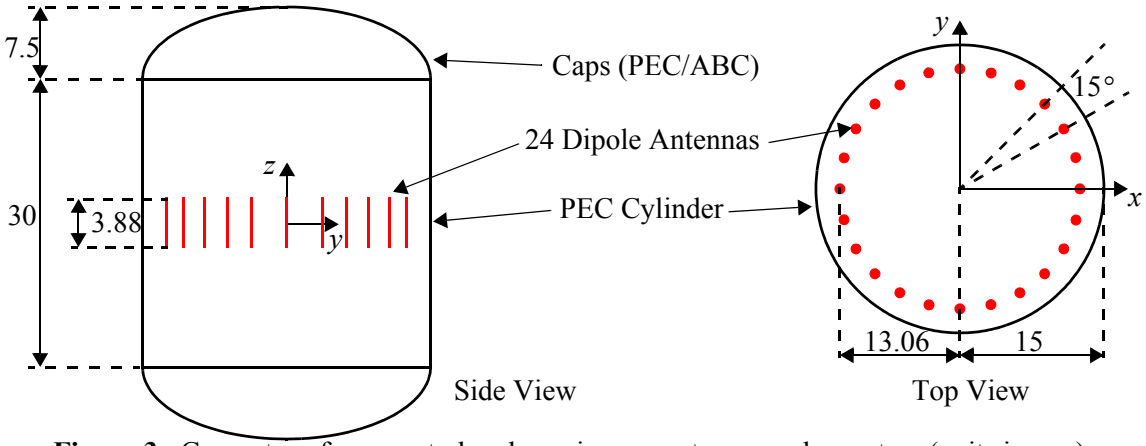

Figure 3. Geometry of resonant-chamber microwave tomography system (units in cm.).

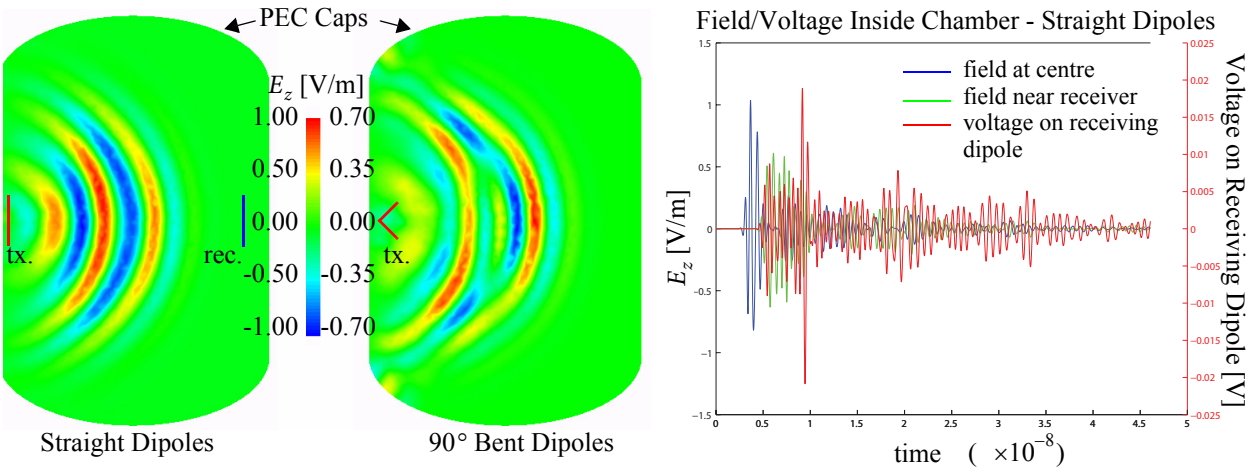

Figure 4. Fields and voltages inside resonant-chamber tomographic system.

resistively-loaded dipoles were modeled (the latter using the Wu-King resistivity profile [6, 7]). Simulated E_z-components for a straight and vee-dipole, PEC capped chamber, are compared in Fig. 4. Both dipoles produce relatively clean sinusoidal wavefronts thus yielding flatter frequency domain spatial response (not shown), with similar magnitudes. Asymmetries in the vee-dipole plot (Fig. 4) are due to asymmetries in the unstructured mesh used in the model. The advantages of using the vee-dipole or the resistive loading have not been thoroughly investigated. The $E_z(t)$-component has also been plotted at two different positions in the chamber and compared to the induced voltage on the diametrically opposite receiving antenna (Fig. 4).

4. Conclusion

A thin-wire model has been introduced for the FVTD algorithm. The advantages are that the thin wires do not need to be resolved in the tetrahedral mesh. The algorithm has been validated on several test problems and the preliminary investigation of a resonant chamber MWT system excited by thin-wire dipoles has been presented. We will continue to use our FVTD tool for the future MWT system development we are undertaking, as well as to generate synthetic data for our imaging studies.

5. References

[1] P. Bonnet, X. Ferrieres, P.L. Michielsen, P. Klotz "Finite volume time domain method," in *Time Domain Electromagnetics,* S.M. Rao (editor), pp. 307-367, Academic Press, San Diego, 1999.

[2] F. Edelvik, G. Ledfelt, P. Lötstedt, D.J. Riley "An unconditionally stable subcell model for arbitrarily oriented thin wires in the FETD method," *IEEE Trans. AP*, vol. 51**,** no. 8, pp. 1797-1805, Aug. 2003.

[3] F. Edelvik "A new technique for accurate and stable modeling of arbitrarily oriented thin wires in the FDTD method," *IEEE Trans. EMC*, vol. 45, no. 2, pp. 416-423, May 2003.

[4] D. Firsov, J. LoVetri, I. Jeffrey, V. Okhmatovski, C. Gilmore, W. Chamma "High-order FVTD on unstructured grids using an object-oriented computational engine," *ACES Journal*, vol. 22, no. 1, pp. 71-82, March 2007.

[5] R. Holland, L. Simpson "Finite-difference analysis of EMP coupling to thin struts and wires", *IEEE Trans. EMC*, vol. 23, no. 2, pp. 88-97, May 1981.

[6] T. T. Wu, R. W. P. King "The cylindrical antenna with nonreflecting resistive loading" *IEEE Trans. AP*, vol. 13, no. 3, pp. 369-373, May 1965: Corrections, vol. 13, no. 6, p. 998, Nov. 1965.

[7] J.G. Maloney, G.S. Smith "A study of transient radiation from the Wu-King resistive monopole-FDTD analysis and experimental measurements," *IEEE Trans. AP*, vol. 41, no. 5, pp. 668-676, May 1993.